UNIVERSITY OF LEEDS

This is a repository copy of *Structural, Spectroscopic, and Excitonic Dynamic Characterization in Atomically Thin Yb3+-Doped MoS2, Fabricated by Femtosecond Pulsed Laser Deposition*.

White Rose Research Online URL for this paper:
http://eprints.whiterose.ac.uk/150678/

Version: Accepted Version

Article:
Maddi, C orcid.org/0000-0003-0454-776X, Aswin, JR, Scott, A orcid.org/0000-0003-4235-6462 et al. (4 more authors) (2019) Structural, Spectroscopic, and Excitonic Dynamic Characterization in Atomically Thin Yb3+-Doped MoS2, Fabricated by Femtosecond Pulsed Laser Deposition. Advanced Optical Materials, 7 (21). 1900753. ISSN 2195-1071

https://doi.org/10.1002/adom.201900753

© 2019 WILEY-VCH Verlag GmbH & Co. KGaA, Weinheim. This is the peer reviewed version of the following article: Maddi, C., Aswin, J. R., Scott, A., Aslam, Z., Willneff, E., Adarsh, K. N. V. D., Jha, A., Structural, Spectroscopic, and Excitonic Dynamic Characterization in Atomically Thin Yb3+-Doped MoS2, Fabricated by Femtosecond Pulsed Laser Deposition. Adv. Optical Mater. 2019, 7, 1900753. https://doi.org/10.1002/adom.201900753 , which has been published in final form at https://doi.org/10.1002/adom.201900753. This article may be used for non-commercial purposes in accordance with Wiley Terms and Conditions for Use of Self-Archived Versions. Uploaded in accordance with the publisher's self-archiving policy.

Reuse
Items deposited in White Rose Research Online are protected by copyright, with all rights reserved unless indicated otherwise. They may be downloaded and/or printed for private study, or other acts as permitted by national copyright laws. The publisher or other rights holders may allow further reproduction and re-use of the full text version. This is indicated by the licence information on the White Rose Research Online record for the item.

Takedown
If you consider content in White Rose Research Online to be in breach of UK law, please notify us by emailing eprints@whiterose.ac.uk including the URL of the record and the reason for the withdrawal request.

White Rose university consortium
Universities of Leeds, Sheffield & York

eprints@whiterose.ac.uk
https://eprints.whiterose.ac.uk/

Structural, Spectroscopic, and Excitonic Dynamic Characterisation in atomically thin Yb^{3+} -doped MoS_2, fabricated by femtosecond pulsed laser deposition

Chiranjeevi Maddi[1], Aswin J R [2], Andrew J Scott [1], Zabeada Aslam[1], Elizabeth A Willneff [3], Adarsh K. V [2+], Animesh Jha[1*]

[1]School of Chemical and Process Engineering, Faculty of Engineering, University of Leeds, Leeds LS2 9JT, UK

[2]Department of Physics, Indian Institute for Science Education and Research (IISER), IISER Bhopal, India

[3]School of Design, Faculty of Arts, Humanities and Cultures, University of Leeds, Leeds LS2 9JT UK

Corresponding Authors[*+]

[*]Email: a.jha@leeds.ac.uk

[+]Email: kv.adarsh@gmail.com

ORCID

Chiranjeevi Maddi: 0000-0003-0454-776X

Andrew J Scott: 0000-0003-4235-6462

Adarsh KV: 0000-0002-6337-6545

Animesh Jha: 0000-0003-3150-5645

Keywords:

molybdenum disulfide, rare-earth ion photoluminescence, femtosecond pulsed laser deposition, saturable absorber, nonlinear optical properties

Abstract

We demonstrate for the first time the large area deposition and synthesis of 10mmx10mm atomically thin Yb^{3+}-doped MoS_2 films by femtosecond pulsed laser deposition on a silica glass optical platform for device applications. The presence of Yb^{3+}-ion doping was confirmed using photoluminescence (PL), X-ray photoelectron spectroscopy (XPS) and Raman spectroscopy. The PL studies using a 976 nm laser demonstrated the Yb^{3+}-ion emission peak in MoS_2 films at ~1002 nm arising via the $^2F_{5/2}$-$^2F_{7/2}$ transition, which was absent in the undoped films. The XPS and Raman spectroscopic analyses of the Yb^{3+}-doped and undoped films showed that the deposited films were a mixture of 2H- and 1T-MoS_2 after post-deposition annealing at 500^{o}C. The Density Functional Theory analysis showed that the 1T phase was metastable by +77kJ (~0.8eV)/mole, when compared with the 2H state at 0 K. Ultrafast nonlinear optical measurements proved that the saturable absorption of undoped MoS_2 was significantly modified after Yb^{3+}-ion doping, by displaying dopant-host structure charge transfer which was characterised by ultrafast transient absorption spectroscopy. The complex transient absorption line shape showed a combination of bleach (negative) signals at the A (670 nm) and B (630 nm) exciton energies, and a strong induced absorption below the A exciton level. The results presented herein provide critical insight in designing novel rare-earth-ion doped 2D materials and devices. (214 words)

1. Introduction

Atomically-thin MoS_2 is recognized as a potential material for next generation of optoelectronic devices, exhibiting quantum phenomena due to its unique electronic structure, mainly because of the confined and reduced symmetry. For example, in monolayer MoS_2, the intrinsically broken crystal inversion symmetry allows the generation of degenerate valley-selective electrons in the K and K' valleys in momentum space locked by time-reversal symmetry.[1],[2] Reduced dielectric screening of atomically thin MoS2 allows to form highly stable neutral and charged excitons even at room temperature with the binding energies many orders of magnitudes higher than conventional Ga, In and As based 2D materials [3],[4] . The charge transfer properties offer opportunities for optoelectronic device applications, for example, n-type doping in MoS_2 by coupling with a charge transfer complex of aromatic benzyl viologen.[5] Similarly, the donor-acceptor charge transfer between $MoSe_2$ and graphene oxide has been shown to enhance the nonlinear absorption by as much as 30 times.[6] By contrast, doping of MoS_2 with rare-earth ions may enhance absorption and emission of near-IR photons, in which the energy transfer may be mediated through the intrinsic defect states of MoS_2 films. Such energy transfer mechanisms might provide high photon yields via quantum cutting in the intra 4f-electronic transitions, as shown elsewhere for photoluminescence and laser characterisation in Tm^{3+}-doped Si thin films[7] and waveguide gain medium,[8] respectively. Although, the spectroscopic and structural studies on chemical vapour deposited Er^{3+}-doped MoS_2 thin-films [ ] for demonstrating near-IR (800nm and 1550 nm) and visible emissions using blue laser source at 488 nm [ ] has been demonstrated, however for optical and data communication devices, most Er^{3+}-doped devices utilise the near-IR pumping scheme to make system engineering compatible

with low-cost fibre coupled semiconductor pump sources at 940-980nm.. For enabling potential applications of MoS_2 photonic devices on silicon and silica planar platforms using femtosecond pulsed laser deposition (fs-PLD) [,], we have chosen Yb^{3+}-ion doping of MoS_2 films for enabling low-cost 980 nm fibre or planar-circuit integrated pumping scheme which will offer significant benefits for optical communication and mid-IR device engineering. The other main advantage of Yb^{3+}-ion doping is the resonant overlap of its 2-level ground state ($^2F_{5/2}$ and $^2F_{7/2}$) transition at ~1 eV, which overlaps with the bandgap of silicon for energy transfer in PV devices for energy harvesting. Photoluminescence (PL) studies using a 976 nm diode laser source reveal that the doped MoS_2 films show room temperature emission centred at ~1002 nm, originating from the optical transition between above-ground states, Yb^{3+} $^2F_{5/2}$ to $^2F_{7/2}$ level. By comparison, absence of the PL in atomically thin undoped MoS_2 is possible pumping via A and B exciton bands centred around 670 and 630 nm, respectively.[9],[10] The ultrafast transient absorption (TA) data present the direct evidence of the charge transfer states in RE-doped atomically thin MoS_2, which are relevant for saturable absorbers and optical switching, in lasers and isolators, respectively.

Since a majority of rare-earth sulphides have high melting and boiling points, the doping of RE^{3+}-ions via chemical vapour deposition is non-trivial, as in the case of solution methods. It is for this reason in this investigation we have adopted femto second pulsed laser deposition, which aligns well with multi target use for in situ mixing in the ablation plasma during deposition. By adopting fs-PLD, we demonstrate the fabrication of nearly 2 nm atomically thin Yb^{3+}-doped MoS_2 , in which a Ti-sapphire laser was tuned to operate at 800 nm with 10Hz-1kHz repetition rate. The optimized and precise control of ablation rate of target permits the growth of atomically thin MoS_2

layers, as shown herein without compromising the stoichiometry. The fs-PLD approach demonstrated is based an earlier report on fs-PLD of Tm^{3+}-doped Si films for waveguide fabrication.[7] Together with the control of deposition parameters, namely the substrate temperature, chamber pressure and rastering of fs-pulsed laser on the target, we were able to fabricate 2-5 nm Yb^{3+}-doped MoS_2 of uniform thickness over a large area of 10mmx10mm on silica glass substrates, which may then allow in the future growth of such films of uniform thickness on a larger surface for photonic and optoelectronic device applications. In an earlier report on nano-second excimer PLD, using Er^{3+}-ion doped glass and poly dimethyl silane targets,[11] multilayer glass-polymer superlattice growth was demonstrated for waveguide fabrication. Our vision for future is to use multiple targets e.g. carbon for graphene and other types of di-metal chalcogenide for engineering atomic layer growth of films, in the way as has been achieved for the III-V and II-VI semiconductor heterostructures.

The complementary structural, spectroscopic, and excitonic characterisations are also included for exploring opportunities for engineering materials using fs-PLD via control of phase transformation from 1T to 2H phase in MoS_2, transient absorption measurements of excitons for engineering saturable absorber and ultrafast detectors in visible, near-IR and mid-IR, and long-lived rare-earth ion doped 2D devices for photon generation.

2. RESULTS AND DISCUSSION

Figure 1(a) shows the cross-section of a focussed ion beam prepared transmission electron microscope (TEM) image of a 2nm atomically thin Yb^{3+}-doped MoS_2,deposited on silica, . which is intermittently discontinuous due to the low deposition temperature maintained at 500^{o}C. The nano-scale discontinuity is more evident in

Figure 1a, next to the silica substrate, which in the subsequent layers become more continuous as the MoS_2 layers grow away from the silica substrate. Figure 1(b) compares a typical vibrational spectroscopic structure of semiconducting trigonal 2H-phase in undoped and Yb^{3+}-doped MoS_2, with two characteristic intense Raman peaks at 382 cm^{-1} and 405 cm^{-1} corresponding to the E^1_{2g} and A_{1g} vibrations, respectively for in-plane symmetric stretching of Mo^{4+} and S^{2-} ions and out-of-plane vibration of S^{2-} ions of crystalline 2H-MoS_2.[10] From the frequency difference of 23.5 cm^{-1} between the two vibrational modes, it is estimated that the overall thickness of the deposited film is between 3 and 4 layers of MoS_2[12], [13],[14], which was found to be consistent with the TEM microscopic analysis, shown in Figure 1(a). Up to 5 nm thickness of MoS_2 films were also grown on silica substrate, for which the Raman spectroscopic data are compared in Figure (S1a) in the Supplementary Information. For characterising the uniformity of deposited Yb^{3+}-doped and undoped thin films of MoS_2, the Raman spectroscopic analysis was carried out at the left, right and centre of films with 10mmx10mm surface coverage, as shown in Supplementary Information Figure (S1b). Both the large area (10x10 mm^2) and point-by-point Raman spectroscopy data confirm that the films were uniform with approximately 3 to 4 layers of MoS_2. Figures 1(b) and (S1b) show that both the Raman spectra of undoped and doped films are asymmetrically broadened, which may be attributed to the lack of extended 2D-order in films due to the stochastic nature of fs-PLD, even at 500^{o}C, when compared with more epitaxial growth.[15] The second reason for asymmetry in Raman peak may arise as a consequence of the introduction of octahedral distortion due to the presence of Yb^{3+}-ions, which have a preferential 6-fold symmetry with S^{2-} anions.[16] The small red-shift in the Raman peaks for the E^1_{2g} and A_{1g} vibration modes may be attributed due to temperature dependent relaxation of MoS_2 layers [12a], which was also reported

earlier in the case of Er^{3+}-doped films [Bai et al]. In addition to the E^1_{2g} and A_{1g} modes, three disorder peaks were fitted (Figure 1b inset), which originate from the transverse optical (378 cm^{-1}), longitudinal optical (370 cm^{-1}), and out of plane optical branches (414.5 cm^{-1}) at the M point of the Brillouin zones. The large integrated intensities of these modes, compared to the E^1_{2g} and A_{1g} modes, indicate the presence of local disorder or lack of continuum of structure in the deposited films, which might be due to the low deposition temperatures.[17];[18]. The temperature-dependent change in the E^1_{2g} and A_{1g} Raman peaks, however, was found to be symmetrical. The second reason for asymmetry is likely to be due to the incorporation of octahedrally co-ordinated Yb^{3+}-ions into the layered MoS_2 structure[19]. The structural change in the ionic co-ordination of MoS_2 in the 2H-type pyramid structure may be expected due to the presence of 6-fold co-ordinated Yb^{3+}-ions, which is heavier (173.04 amu for Yb) than Mo^{4+}-ion (95.94 amu for Mo) in 2H-type MoS_2. The changes in ionic co-ordination and atomic mass may therefore introduce vibrational anharmonicity due to the changes in the Coulombic force (i.e. the spring constant in the linear harmonic oscillator), which is why the Raman peaks appear asymmetrically broad in Figures 1b and S1b. Consequently, the Raman peaks shift to lower energy with respect to the undoped peak.

The chemical composition of the deposited MoS_2 was investigated by X-ray photoelectron spectroscopy (XPS). Figure 1(c) shows a comparison of Yb- $4d_{5/2}$ core level spectra of the undoped and doped MoS_2 films. Yb^{3+} ions are clearly present in the 2nm thick doped MoS_2 film. This is confirmed by the binding energy of Yb-$4d_{5/2}$ peak at 185.3±0.5 eV which is consistent with the Yb being in the 3+ oxidation state with a sulphur coordination shell [20];[21], with concentration of Yb^{3+}-ions around 1 ion%. For comparison, the core level spectra of molybdenum (Mo) and sulphur (S) are also

presented in Figure S2 (supporting information). From the comparison of molybdenum core-level data for doped and undoped MoS_2 thin films herein with the literature data on Er^{3+}-doped films [Bai et al], it is evident that the doping with Yb^{3+}-ions has led to a shift in the peak energies (Mo $3d_{5/2}$).

Figure 1d compares the UV-visible absorption spectra for the Yb^{3+}-ion doped and undoped MoS_2 films, from which it is evident that the background loss in 2 nm thick films of MoS_2 increases with doping, which may be due to the following reasons. In the fs-deposited films the octahedral crystal field distortion of Yb^{3+}-ions perturbs the structural continuity of the 10x10mm^2 2D-films and may be contributing to the Rayleigh-scale scattering. The second reason may be due to the increased concentrations of carrier states, contributing to the overall absorption which is likely due to the difference in the charge on Yb^{3+} and Mo^{4+} ions, creating a donor level in the MoS_2 lattice. The UV-visible spectra in Figure 1d (and the 2nd derivative spectra in the inset) of doped and undoped films reveal two absorption peaks at 620 nm and 670 nm, corresponding to the B and A excitonic bands, respectively originating from the doubly degenerate valence band of Mo^{4+}-ion.

Following the structural and chemical characterizations, the room temperature photoluminescence studies on Yb^{3+}-doped and undoped MoS_2 thin films were carried out using a 976nm laser diode as an excitation source. The room temperature PL of Yb^{3+}-doped MoS_2 is shown in Figure 2a and the PL of the Yb^{3+}-doped film compares well with the data in literature [22];[23] on crystals and glass materials. Considering the apparent small volume of film on a 2nm scale and the resulting influence of inhomogeneous broadening of the PL line shape, the full-width-of-half maximum (FWHM) of the optical transition: $^2F_{5/2} \rightarrow {}^2F_{7/2}$ is less than 12nm with the emission peak centred at 1002nm, which is in reasonable agreement with the 70-80nm FWHM data

in bulk materials. The apparent reduction in FWHM to 12 nm in a 2 nm thick Yb^{3+}-doped MoS_2 appears to be due to the confined dimensions of the film. In Figure 2b, the apparent shifts towards lower energies, observed in the Mo-3d core level XPS spectra for Yb^{3+}-ion doped films are compared with the undoped films, and the apparent shifts are consistent with data for Er^{3+}-ion doped MoS_2 [ ]. Further detailed analysis are included in Figure S2 and Table S1 in SI.

In this experimental analysis of fs-pulsed laser deposited films, formed via ablation and plasma relaxation in the sub-nano to pico second regime, the influence of sub nano second time scale deposition on the phase transformation on 2H to 1T phase transformation in undoped MoS_2 structures has also been further investigated. Since the DFT characterisation of low dimension Yb^{3+}-doped film is non-trivial and requires more explanation, it is excluded in this article and will be published separately by emphasizing the phase transformation in doped materials. For this reason, the DFT calculations have been performed using the pseudopotential code, Castep[24] on both the 2H-MoS_2 and the metastable 1T-MoS_2 structures. The bulk structures were geometry optimised using the dispersion corrected TS-GGA-PBE functional[25] which ensures that the weak interlayer forces are correctly described. A kinetic energy cut-off of 490 eV and a k-point mesh of 0.02 $Å^{-1}$ was used to ensure high precision with a force convergence tolerance of 0.01 eV $Å^{-1}$. The energy minimised lattice parameters are shown in Table S2. Note that the DFT optimises the structures at zero Kelvin. A comparison is made in which, the experimental 2H-MoS_2 being an extrapolation to 0K [26] and the 1T-MoS_2 being the recent room temperature structure determination[27]. The DFT minimised lattice parameters are in excellent agreement with experiment; the expected large expansion coefficient in the direction perpendicular to the interlayer spacing (c-axis) for the 1T-MoS_2 accounts for the 5% deviation between calculated

and experimental c-lattice parameter. The MoS_2 coordination geometries for the 2H (trigonal) and the 1T (octahedral) are shown in Figures S4a and S4b (In supporting file), the Mo-S bond lengths being 2.401 Å and 2.418 Å, respectively. A comparison of the total energies of the optimised structures confirms that the 2H MoS_2 is thermodynamically more stable than the 1T (+76.1 kJ/mol.fu), as shown in Table S2.

It is known that DFT, using standard exchange-correlation functionals, can significantly underestimate the band gap in materials. For 2H-MoS_2 and 1T-MoS_2, further electronic structure calculations were performed with the recent hybrid HSE06 functional [28] which has been demonstrated to give accurate band gaps for a range of materials, albeit with a large increase in computational cost. The DFT results herein show an indirect band gap of 1.3 eV for bulk 2H-MoS_2 and bulk 1T-MoS_2 to be a conductor. In addition, an electronic structure calculation on a monolayer of MoS_2 with the 2H geometry (15Å vacuum in c-axis), showed an opening of the band gap to a direct gap of ~2.3 eV.

From the Raman analysis in Figure 1b, the volume fraction ratio of 2H and 1T phases were ascertained for the doped and undoped MoS_2 films, annealed at 500^{o}C. The literature [12c] data shows that although the annealing stabilizes the 2H-phase, in this study longer annealing time (see SI) at elevated temperature reduce the fractions of 1T phase.

The excitonic dynamic analysis of fs-PLD MoS_2 films are unknown, especially when the deposited films may be a mixture of 2H and 1T phases. For photonic device applications, it is also important that the rare-earth ion dopants (e.g. Yb^{3+}-ions) are incorporated for photon generation by taking advantage of the excitonic states in the materials. After a systematic analysis of structure of the deposited films, the nonlinear optical absorption of atomically thin ~2nm doped and undoped MoS_2 films were

characterized using the conventional open aperture Z-scan method, which helped in the quantitative determination of the total transmittance as a function of incident laser intensity[29];[30]. The normalized Z-scan peaks and the evolution of shapes therein for the Yb^{3+}-doped MoS_2 films are presented in Figure 3a for three on-axis peak intensities at 77, 110 and 156 GW/cm^2. The sub-bandgap excitation was at 800 nm, which is at a higher energy than the above-ground state of Yb^{3+}:$^2F_{5/2}$ in doped MoS_2, from which it is evident that the normalized transmittance of the films at 110 and 156 GW/cm^2 intensities show a gradual increase towards the focal point, by reaching its maximum transmittance value at the Z=0 focal point. However, the films did not show any nonlinear absorption below a threshold peak intensity of 77 GW/cm^2, even though the excitation wavelength at 800 nm was in the 2-photon absorption regime. From Figure 3b for the undoped MoS_2 thin film irradiated at 77, 110, and 156 GW/cm^2, the saturable absorption was apparent at each intensity. Furthermore, the saturable absorption was analyzed and quantified using the Z-scan theory.[31] In the experimental method discussed, the propagation equation may be described as a function of the position as

$$\frac{dI}{dz} = -\alpha(I)I \qquad (1)$$

where $\alpha(I)$ is the intensity dependent absorption coefficient which can be calculated as

$$\alpha(I) = \frac{\alpha_0}{1+\frac{I}{I_S}} + \beta_{TPA}I \qquad (2).$$

Here I_s, β_{TPA} and α_0 are the saturation intensity, two photon absorption coefficient and linear absorption coefficient, respectively. Since it was found that the contribution of β_{TPA} is negligible due to the nanometer scale thickness (z) of thin films, we used the minimum value of β_{TPA} for fitting the experimental data. From the best fit to the normalized transmittance curve, it was found that the saturation intensity (I_s) value for

Yb^{3+}-doped MoS_2 is of the order of 882±58 to 399±20 GW/cm^2 for the peak intensities of 110 and 156GW/cm^2, respectively. By comparison, at these two peak intensities, the values for undoped MoS_2 films were found to be 228±13 GW/cm^2 and 149±06 GW/cm^2, which are much lower than that for the Yb^{3+}-doped thin films. Although 800 nm excitation wavelength lies below the bandgap region of both the undoped and Yb^{3+}-doped MoS_2, in order to explain the observation of ultrafast saturable absorption, a 3-level model with energy transfer for MoS_2 and Yb^{3+}-doped MoS_2 films is proposed for the defect states, valence and conduction bands, as shown in Figure 3c and 3d. The model is further supported by the band structure diagrams for 2H and 1T in Figures S3a and S3b (Supporting file), respectively. The 800 nm excitation creates resonant single photon absorption of carriers from the valence band to the defect state, as shown in Figure 3c. Since the density of defect states are low, typically less than ~10^{18}/cm^3, the defect states are almost occupied when peak intensity increases above 77 GW/cm^2. Consequently, Pauli blocking stops further absorption, which eventually results in saturable absorption. After demonstrating saturable absorption, it is also important to calculate the ground-state (σ_{gs}) and excited-state (σ_{es}) absorption cross-sections, which helps in identifying the mechanism for the 3-level saturable absorption in undoped MoS_2 and occurs when σ_{es} is much smaller than (σ_{gs}).

$$\sigma_{gs} = \frac{-\log T_0}{NL} \quad (3)$$

$$\sigma_{es} = \frac{-\log T_{max}}{NL} \quad (4)$$

where T_0, T_{max}, N, and L are the transmission in the linear regime, high intensity saturated transmission, ground state carrier density and thickness of the saturable absorber for 2nm thick MoS_2 film, respectively. The calculated values of σ_{es} and σ_{gs}

for Yb^{3+}-doped MoS_2 are 1.97×10^{-12} cm^2 and 9.8×10^{-12} cm^2, respectively. From the calculated values of absorption cross-sections, the ratios of σ_{es}/σ_{gs} were found to be 0.75 and 0.50 for the doped and undoped MoS_2, respectively, which point out that the excited state absorption cross-section has increased significantly with Yb^{3+}-ion doping at ~1 ion% by creating a new level in the excited state of MoS_2.

For more in-depth characterisation of the saturable absorption of Yb^{3+}-doped MoS_2 due to the presence of defect states, analysis using ultrafast broadband transient absorption (TA) spectroscopy was performed. In this experiment, Yb^{3+}-doped MoS_2 was excited with 120 fs pulses centred at 400 nm, and the changes in absorption of wavelengths between 525 nm and 735 nm, which overlap with the A and B exciton transitions and defect states, were recorded by using white-light continuum pulses. The TA of the Yb^{3+}-doped and undoped film was mapped in the contour plot shown in Figure 4(a) and Figure 4(b), respectively. It is evident from the transient data that a strong excitonic bleach is observed in doped MoS_2 compared to undoped MoS_2. The cross sections of the contour at different probe delays are compared in Figures 4c and 4d for Yb^{3+}-doped MoS_2 and undoped films, respectively. The complex TA line shape may be better described as a combination of bleach (negative) signals at the A (energy, 1.81 eV) and B (energy, 2.04 eV) exciton energies and a strong induced absorption below the A exciton energy that appears only after the carrier thermalization (300 fs). The energy values and delayed response clearly suggest that these features are originating from the trap and Yb^{3+}-states. To account for the instantaneous bleaching of the excitonic resonances, it was assumed that the electric field produced by the exciton of the pump beam causes the Stark effect on the absorption of the probe beam exciton. In such cases, the spectral signature of the TA closely matches with the second derivative of the ground state absorption spectrum,

i.e. $\Delta A(v) \alpha E^2 A''(v)$, where E and A" are the strength of the electric field and second derivative of the ground state absorption spectrum, respectively as shown in Figure 4d. At the initial timescales, the Coulomb interaction between the excitons blue shift and broaden the excitonic resonance. This is manifested in the TA spectrum as the bleaching signal at the positions of the resonant exciton energy and an induced absorption at the higher energy regions. At this stage, we assume that the contribution from the state filling to the band edge signals are insignificant since the sample was excited with above bandgap, using a 400 nm source, and therefore the band edge states remain unoccupied at the early times. In order to access better insight into the time dependent shift of the exciton resonances due to the correlated exciton interactions, we have carried out the global fitting of the TA using the following equation:

$$\Delta A = \sum_{i=1}^{2} A_i(es) e^{-((x-x_{0i}-\delta_i)/\Gamma_i)^2} - A_i(gs) e^{-((x-x_{0i})/w_i)^2} \quad (5),$$

where δ_i, Γ_i and w_i are the shift in exciton energy due to the exciton-exciton interactions, the FWHM of exciton transition in the excited state, FWHM in the ground state, respectively. $A_i(es)$ and $A_i(gs)$ are the Gaussian functions describing the excited and ground states exciton absorption and '*i*' corresponds to A and B excitons. The solid lines in Figure 4c show the representative fits at each selected Δt using Equation. 5. From this figure, it is evident that the proposed model exactly reproduces the TA spectrum, i.e. bleaching features corresponding to A and B excitons and the absorption feature in between them.

For analysing the dopant-host structure charge transfer of defect and Yb^{3+}-ion states, we have examined the lower-energy part of ΔA spectrum because their contribution is more pronounced below the A exciton resonance energy. Note that the features of

induced absorption in the TA does not disappear even after the complete decay of excitonic bleach (Figure 5(a) and 5(b)), which may be attributed to the defect and Yb^{3+}-ion states related absorption, originating from the re-excitation of band edge carriers captured by these states. These defect states are associated with layer interfaces, grain boundaries and surface defects have already been observed in many theoretical and experimental studies on MoS_2.[15] In Yb^{3+}- doped MoS_2 the saturable absorption bands are much weaker than that in the undoped MoS_2, which may be explicable on the basis of cross-relaxation of defect and excited states, both of which lie higher than the highest sub-Stark state in Yb^{3+}:$^2F_{5/2}$ in the 1-1.025 eV range, as shown in Figure 3c. Note that these absorption bands are much weaker in Yb^{3+}-doped MoS_2, as compared to the undoped MoS_2, which manifest the dopant-host structure charge transfer between the defect and Yb^{3+} states. The characteristics of defects and Yb^{3+}-states can be better understood by the temporal analysis. It is evident from the lifetime of excited carriers in the defect and Yb^{3+}-states that the mΔA curves are not reaching zero even after maximum experimental time window of 1200 ps (Figure 5c), whereas in the undoped films of MoS_2, the relaxation time reaches zero value within 300 ps, as shown in Figure 5d. The delay in the Yb^{3+}: doped MoS_2 film is due to the long lifetimes (100s μs) in undoped MoS_2 Figure. 5(d). Figure 5c and 5d show the temporal evolution of TA, the experimental values are fitted with exponential functions for analysis. The best fit to the experimental data were obtained with decay constants for MoS_2 τ = 16.1 ± 0.4 ps and for Yb^{3+} doped MoS_2 τ = 180 ± 10 ps. Thus, the TA measurements discussed herein provide direct evidence for the presence of defect states and the lifetimes of carriers in such states.

3. CONCLUSIONS

The present investigation demonstrates a first step towards large area (10x10mm^2) deposition of undoped and Yb^{3+}-ion doped MoS_2 films of sub 5-nm scale using near-IR fs-PLD on a silica platform. The deposited MoS_2 films at 500^{o}C on a 2nm scale show a mixture of 2H and 1T-type phases. The phase stability of undoped 1T and 2H MoS_2 phases in bulk and thin film forms were compared using the DFT, and it is evident that the total energies of the optimised structures confirms that the 2H MoS_2 is thermodynamically more stable than the 1T phase. The DFT results also predicts that the thin film 2H geometry showed a direct band gap of ~2.3 eV. The presence of 1T- and 2H-phases were evident from the optical phonon and chemical shifts in Raman and XPS spectra of undoped and Yb^{3+}-doped MoS_2 films, respectively. The film thickness analysis using Raman and cross-sectional TEM were found to be consistent.

The room temperature photo luminescence analysis clearly shows the evidence for photoluminescence with peak at 1002nm, corresponding to the $^2F_{5/2} \rightarrow {}^2F_{7/2}$ optical transition in Yb^{3+}-state. The presence of 1 ion% concentration of Yb^{3+}-ions in the films was confirmed by XPS spectroscopy. The presence of photo-generated excitons and Stark effect due to pump exciton were investigated by analysing the ultrafast transient absorption data. Ultrafast nonlinear optical measurements using 800 nm excitations shows that the saturable absorption of MoS_2 is significantly different when compared with the data for Yb^{3+}:doped MoS_2. The evidence for dopant-host structure charge transfer has been verified with the help of ultrafast pump-probe measurements supported by trap state kinetics. These results suggest that Yb^{3+}-ion doped MoS_2 are promising for optoelectronic applications. Overall, the novel fs-pulsed laser deposition technique may be possible to align with the making 2D-TMS materials on silica and silicon integration platform for photonic devices in future.

Experimental Section

Synthesis of MoS_2 and Yb^{3+}- doped MoS_2 films**:**

Undoped and rare-earth doped MoS_2 films were deposited using a femtosecond pulsed laser deposition (fs-PLD). Before deposition, the PLD chamber was pumped until a base pressure of $<10^{-6}$ Torr. The substrates were carefully cleaned using a two-step process using an ultrasonic bath of acetone and ethanol. After which the substrate was dried and baked inside the deposition chamber under vacuum. A femtosecond laser with a wavelength of 800 nm, pulse duration of 100 fs and repetition rate of 1 kHz was used to deposit the films. The few layers of MoS_2 and Yb^{3+}-doped MoS_2 were deposited under a positive pressure of argon gas, maintained at 10^{-3} Torr. By ablating the pressed pellets of powder materials, MoS_2 and 5% Yb^{3+}-ion% doped MoS_2 targets with fs-PLD, the undoped and doped MoS_2 sub 5 nm films were deposited at 500^{o}C on a silica substrate. The substrates were mounted on a sample holder at a distance of 50 mm from the target. For depositing films on the SiO_2 substrates, the laser fluence used was 3 J/cm^2.[32] After the growth of films, the samples were cooled down from 500^{o}C to room temperature at a rate of 5^{o}C/min. The deposited films were characterized using a range of techniques discussed below and in the article.

Characterization of films:

The undoped and Yb^{3+}-doped MoS_2 thin films were characterized using a Renishaw Raman inVia Microscope, equipped with a laser excitation at 514 nm. A 50x microscope objective with 0.8NA was used. The gratings used in the Raman spectroscopy have a step size of 3-4 microns and a spectral resolution better than 1 cm^{-1}. The laser power was kept below 1 mW to avoid the laser induced degradation of films. The spectral position was calibrated with internal Silicon (Si). The TEM

analysis was carried out using an FEI Tecnai FT 20 Field Emission microscope, operating at 200 kV. The Perkin-Elmer UV-visible-near IR spectrophotometer was used for the characterisation of excitonic absorption bands in the films. XPS spectra were acquired using a SPECS system with high intensity XR50 X-ray monochromatic Al Kα (1486.5 eV) source, and a PHOBIOS hemispherical electron analyser with a pass energy of 30 eV under vacuum of 10^{-10} Torr. Curve fitting was performed using Casa XPS software and energy calibrated to the C 1s peak at 284.6 eV, employing Gaussian-Lorentzian peak shapes and a Shirley background.

Nonlinear optical properties of undoped and Yb^{3+}doped MoS_2 were studied using the open aperture Z-scan technique where the exciting pulsed laser is centred at 800 nm and 120 fs pulse. The exciting beam was focused by a plano-convex lens of focal length 20cm. The sample was moved along the z-axis of the beam by using a computer controlled translation stage. The Rayleigh length (z_0) and the beam waist were 11 mm and 42 μm respectively. During irradiation with ultrashort pulses the repetition rate of the laser is maintained at 1 kHz, so that the radiation induced heating and associated structural changes in the films were negligible. To calculate the excitonic lifetime, the ultrafast transient absorption pump-probe spectroscopic analysis was performed where the pump was centred at 400 nm and probe range was chosen to cover both A and B-exciton studies. Amplifier output of 120 fs pulse width centred at 800 nm fall on a BBO crystal to generate the second harmonic of 800nm (i.e, 400 nm). 400 nm pulsed laser acts as the pump and 800 nm laser falls on a CaF_2 crystal to generate white light which acts as a probe. There is a software controlled delay stage which generates pump-probe delay.

Supporting Information

The supporting information section includes the supplementary Raman, XPS, DFT and Z-scan nonlinear data.

ACKNOWLEDGEMENTS

The authors would like to acknowledge UKIERI-UGC for financial support. C.M and A.J would like to acknowledge EU-Horizon H2020 fellowship. The authors are thankful to J. Harrington and S. Micklethwaite for TEM measurements. This work was undertaken on ARC2, part of the High Performance Computing Facilities at the University of Leeds, UK.

Conflict of Interest

The authors declare no conflict of interest.

Figure 1:

(a)

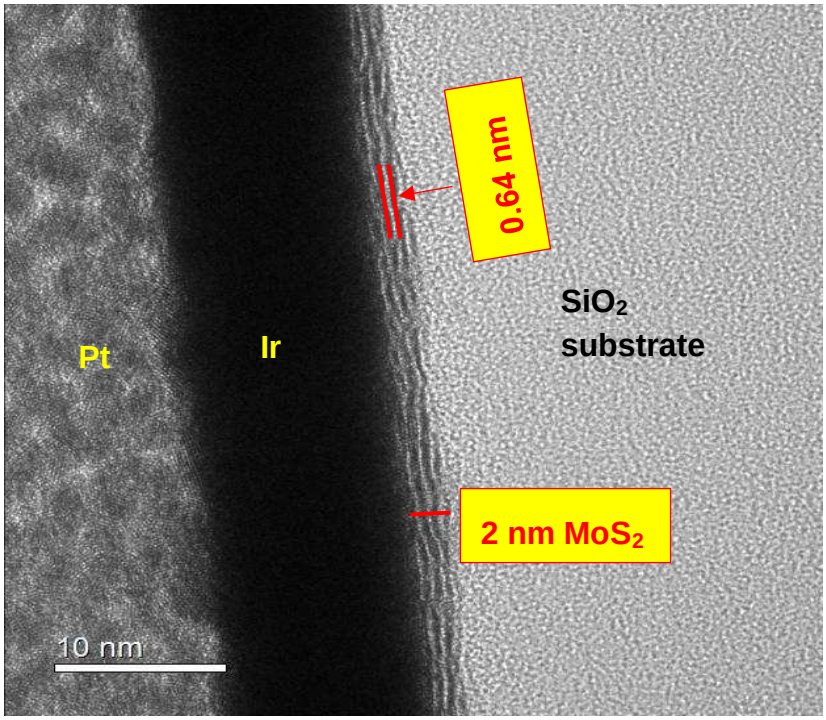
0.64 nm
SiO_2
substrate
Pt
Ir
2 nm MoS_2
10 nm

(**b**)

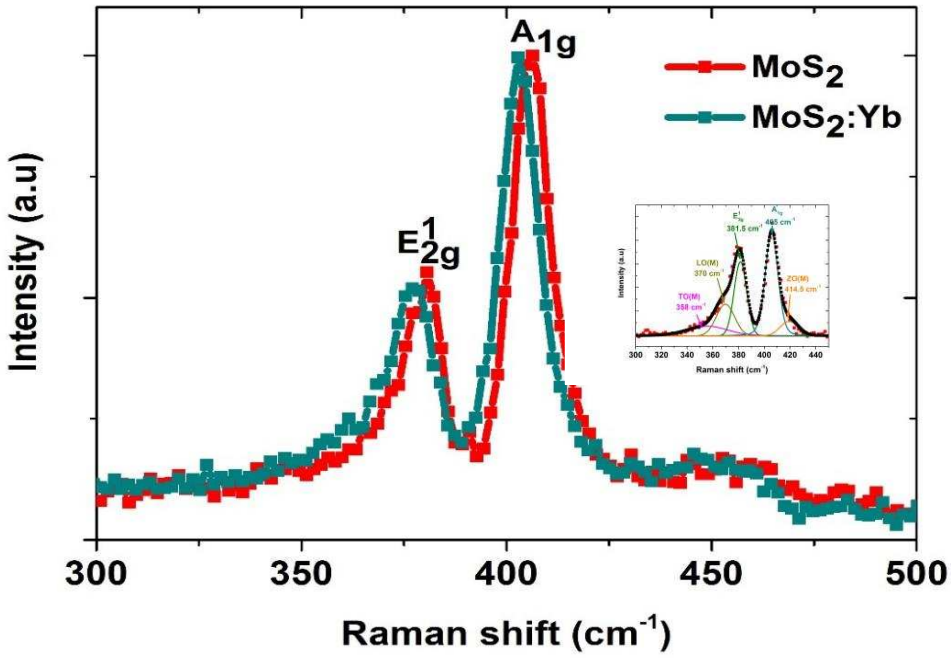
A_{1g}
E^1_{2g}
MoS_2
MoS_2:Yb
Intensity (a.u)
300
350
400
450
500
Raman shift (cm^{-1})

(**c**)

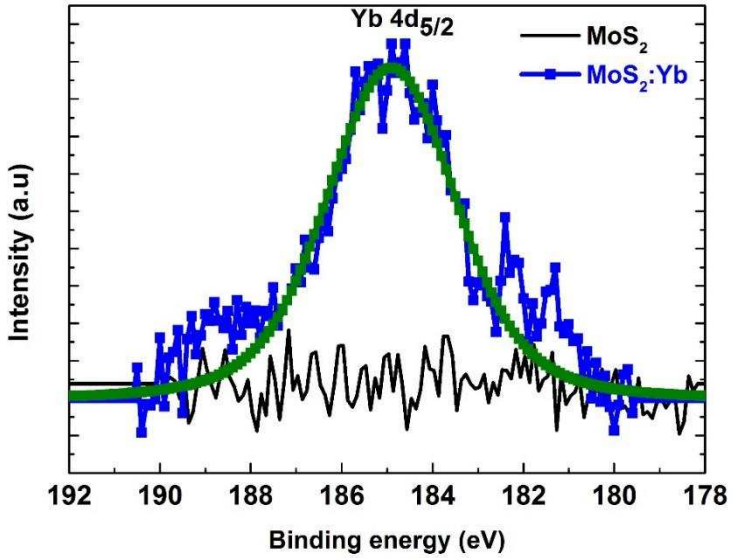

(**d**)

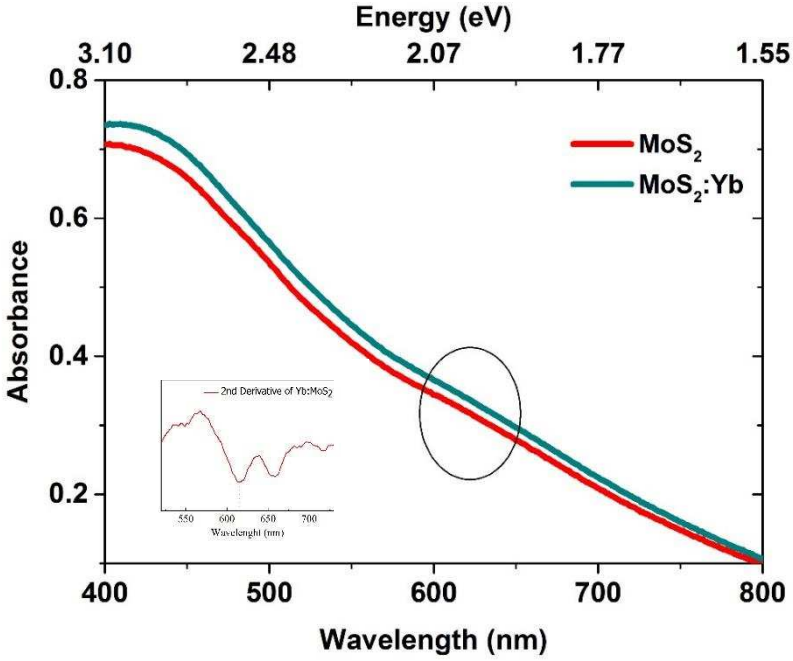

Figure. 1. **(a)** Cross-sectional TEM image of discontinuous MoS_2 film with the evidence for island formation at the SiO_2-MoS_2 interface; a comparison of **(b)** Raman spectra of undoped and Yb^{3+}-doped MoS_2, showing a marginal shift in the peak positions of A_{1g} and E^1_{2g} to lower energies as a result of Yb^{3+}-ion incorporation. The inset shows the fitted optical phonon vibrational modes. **(c)** XPS core level spectra of Yb^{3+}-4d of undoped and doped MoS_2; **(d)**

Optical absorption spectra of Yb^{3+}-doped and undoped MoS_2, shown by a small hump in the 620-630 nm region. The second-derivative of ground state optical absorption was shown in inset.

Figure 2:

(**a**)

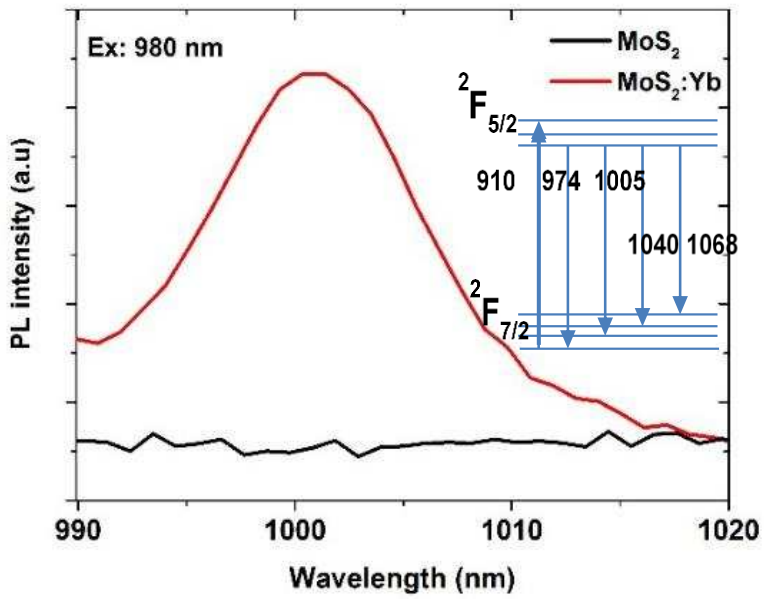

(b)

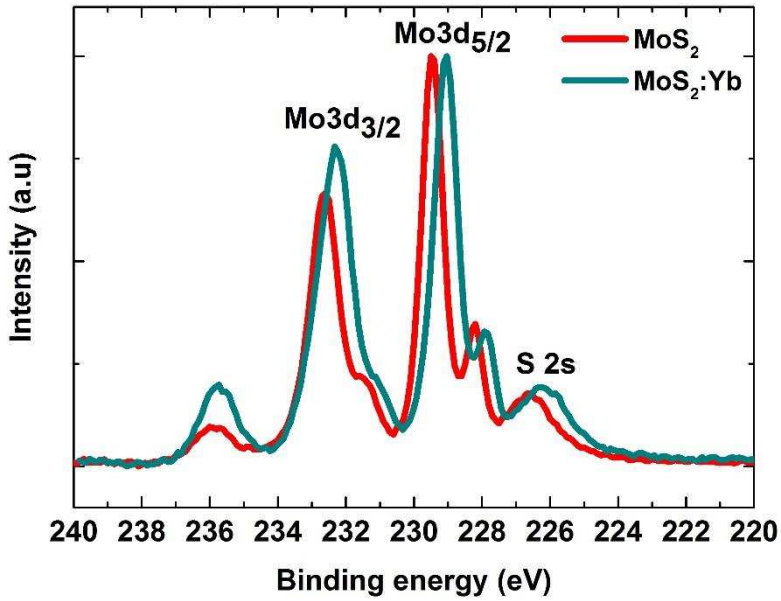

Figure 2: a) Room temperature photoluminescence spectrum of Yb^{3+}-doped MoS_2 thin film using 976 nm excitation source. The inset shown the energy level diagram of Yb^{3+}-ions with $^2F_{7/2}$ ground state and above ground $^2F_{5/2}$. The excitation wavelength may vary between 900 nm to 976, with corresponding Stokes shifted emission lines at longer wavelengths. The apparent observation of room temperature PL is consistent with the energy level diagram. b) Compares the core level XPS data for doped and undoped films, showing that the Yb^{3+}ion doping results into a uniform shift towards lower binding energies. (Figure S2 provides supplementary details and data in Table 2S).

Figure 3:

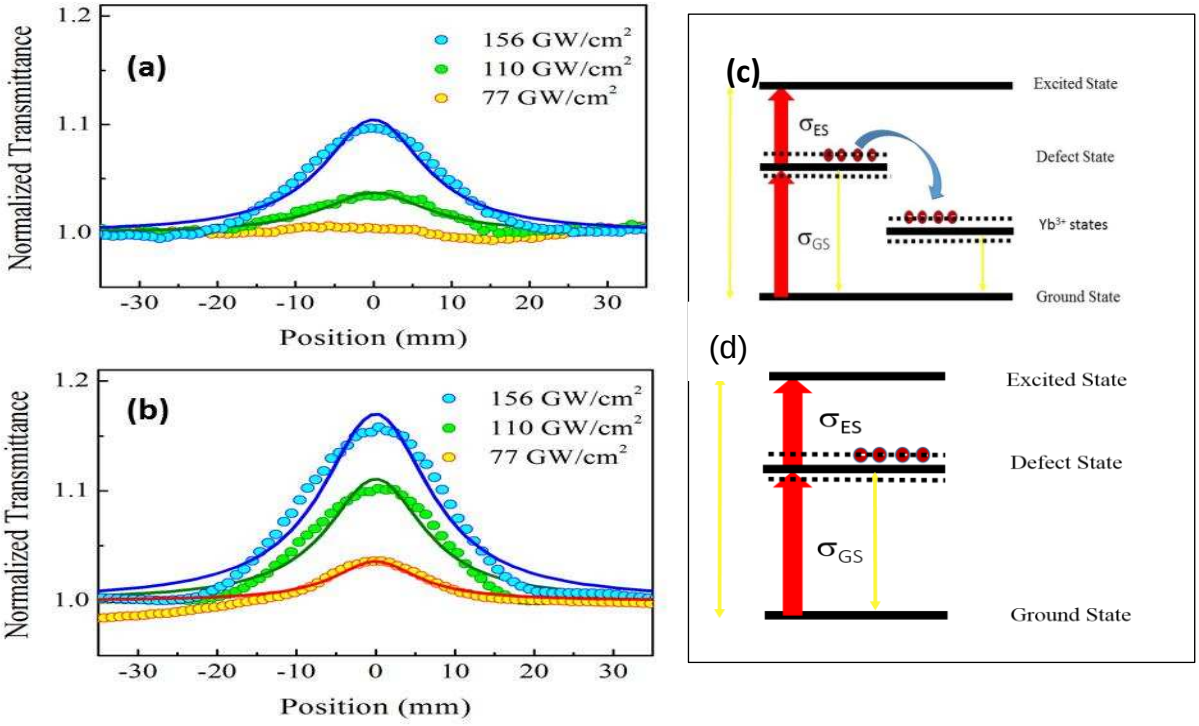

Figure. 3 (a) Normalized transmittance as a function of position in open-aperture Z scan at 120 fs, 800 nm excitation (a) 2 nm (Yb^{3+};doped MoS_2); (b) 2 nm (undoped MoS_2); and (c)and (d) Energy-level representation showing the transfer of energy from the defect and excited states to the Yb^{3+}-ions present in the MoS_2 and MoS_2 films which will lead to diminution in apparent saturable absorption, via the Yb^{3+}:$^2F_{5/2}$-$^2F_{7/2}$ optical transition.

Figure 4:

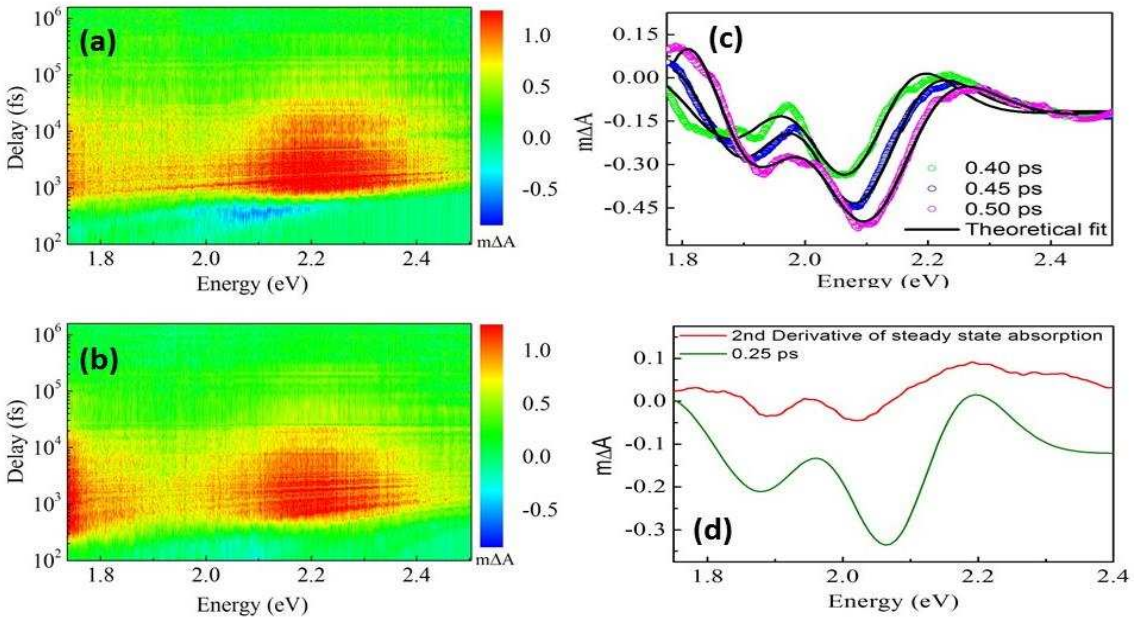

Figure. 4 (a) The Contour plot of TA (transient absorption) spectrum Yb^{3+} doped MoS_2 and (c) undoped MoS_2 thin film when excited with pump pulses at 400 nm. (c) Cross sections of contour plot of Yb^{3+} doped MoS_2 at selected pump probe delays. Here the solid lines represent the global fit using Eq. 1. (d) Comparison of the second-derivative of ground state optical absorption and TA at selected pump-probe delay of Yb^{3+} doped MoS_2.

Figure 5:

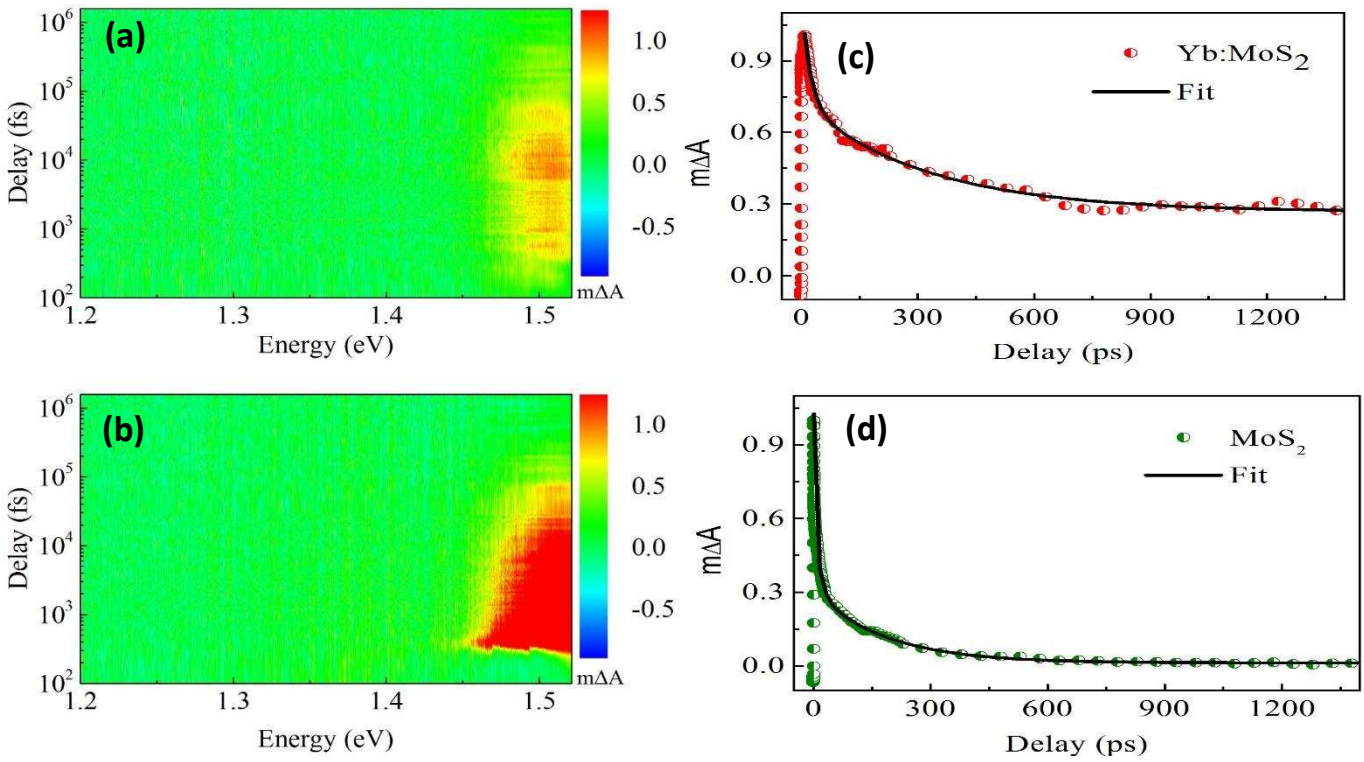

Figure. 5. Contour plot of TA spectrum for trap state kinetics at 1.5 eV for (a) 2 nm doped MoS_2 (b) 2 nm MoS_2. The decay kinetics at 1.5 eV (the temporal evolution of TA) at 826 nm for (c) 2 nm doped MoS_2 (d) 2 nm MoS_2.

References:

[1] A. Steinhoff, M. Florian, A. Singh, K. Tran, M. Kolarczik, S. Helmrich, A. W. Achtstein, U. Woggon, N. Owschimikow, F. Jahnke, X. Li, Nature Physics **2018**, 14, 1199.

[2] L. Sun, C.-Y. Wang, A. Krasnok, J. Choi, J. Shi, J. S. Gomez-Diaz, A. Zepeda, S. Gwo, C.-K. Shih, A. J. N. P. Alù, **2019**, 13, 180.

[3] A. Raja, A. Chaves, J. Yu, G. Arefe, H. M. Hill, A. F. Rigosi, T. C. Berkelbach, P. Nagler, C. Schüller, T. Korn, C. Nuckolls, J. Hone, L. E. Brus, T. F. Heinz, D. R. Reichman, A. Chernikov, Nat Commun **2017**, 8, 15251.

[4] T. Mueller, E. J. n. D. M. Malic, Applications, **2018**, 2, 29.

[5] D. Kiriya, M. Tosun, P. Zhao, J. S. Kang, A. Javey, Journal of the American Chemical Society **2014**, 136, 7853.

[6] R. Sharma, J. Aneesh, R. K. Yadav, S. Sanda, A. R. Barik, A. K. Mishra, T. K. Maji, D. Karmakar, K. V. Adarsh, Phys Rev B **2016**, 93, 155433.

[7] M. Murray, T. T. Fernandez, B. Richards, G. Jose, A. Jha, Applied Physics Letters **2012**, 101, 141107.

[8] F. Fusari, A. A. Lagatsky, G. Jose, S. Calvez, A. Jha, M. D. Dawson, J. A. Gupta, W. Sibbett, C. T. A. Brown, Opt. Express **2010**, 18, 22090.

[9] A. Splendiani, L. Sun, Y. Zhang, T. Li, J. Kim, C.-Y. Chim, G. Galli, F. Wang, Nano Letters **2010**, 10, 1271.

[10] G. Eda, H. Yamaguchi, D. Voiry, T. Fujita, M. Chen, M. J. N. l. Chhowalla, **2011**, 11, 5111.

[11] Z. Zhao, G. Jose, T. T. Fernandez, T. P. Comyn, M. Irannejad, P. Steenson, J. P. Harrington, M. Ward, N. Bamiedakis, R. V. Penty, I. H. White, A. Jha, Nanotechnology **2012**, 23, 225302.

[12] H. Li, Q. Zhang, C. C. R. Yap, B. K. Tay, T. H. T. Edwin, A. Olivier, D. Baillargeat, Adv Funct Mater **2012**, 22, 1385.

[13] B. Chakraborty, H. S. S. R. Matte, A. K. Sood, C. N. R. Rao, **2013**, 44, 92.

[14] S. Sahoo, A. P. Gaur, M. Ahmadi, M. J.-F. Guinel, R. S. J. T. J. o. P. C. C. Katiyar, **2013**, 117, 9042.

[15] A. M. van der Zande, P. Y. Huang, D. A. Chenet, T. C. Berkelbach, Y. You, G.-H. Lee, T. F. Heinz, D. R. Reichman, D. A. Muller, J. C. Hone, Nature Materials **2013**, 12, 554.

[16] A. Well, Structural Inorganic Chemistry, Clarondon press, Oxford **1962**.

[17] S. Mignuzzi, A. J. Pollard, N. Bonini, B. Brennan, I. S. Gilmore, M. A. Pimenta, D. Richards, D. Roy, Phys Rev B **2015**, 91.

[18] M. Mattinen, T. Hatanpää, T. Sarnet, K. Mizohata, K. Meinander, P. J. King, L. Khriachtchev, J. Räisänen, M. Ritala, M. J. A. M. I. Leskelä, Adv Mater Interfaces **2017**, 4, 1700123.

[19] A. F. Wells, Structural Inorganic Chemistry, Oxford University Press, Oxford **1962**.

[20] R. J. Iwanowski, J. W. Sobczak, Z. Kalinski, Acta Physica Polonica Series A **1997**, 91, 809.

[21] P. Ramasamy, P. Chandra, S. W. Rhee, J. Kim, Nanoscale **2013**, 5, 8711.

[22] N. V. Kuleshov, A. A. Lagatsky, V. G. Shcherbitsky, V. P. Mikhailov, E. Heumann, T. Jensen, A. Diening, G. Huber, Applied Physics B **1997**, 64, 409.

[23] K. Lu, N. K. Dutta, Journal of Applied Physics **2002**, 91, 576.

[24] J. Clark Stewart, D. Segall Matthew, J. Pickard Chris, J. Hasnip Phil, I. J. Probert Matt, K. Refson, C. Payne Mike, in Zeitschrift für Kristallographie - Crystalline Materials, Vol. 220, 2005, 567.

[25] A. Tkatchenko, M. Scheffler, Physical Review Letters **2009**, 102, 073005.

[26] R. Murray, B. Evans, Journal of Applied Crystallography **1979**, 12, 312.

[27] Y. Fang, J. Pan, J. He, R. Luo, D. Wang, X. Che, K. Bu, W. Zhao, P. Liu, G. Mu, H. Zhang, T. Lin, F. Huang, Angewandte Chemie International Edition **2018**, 57, 1232.

[28] J. Heyd, G. E. Scuseria, M. Ernzerhof, The Journal of Chemical Physics **2003**, 118, 8207.

[29] M. Sheik-Bahae, A. A. Said, T. Wei, D. J. Hagan, E. W. V. Stryland, IEEE Journal of Quantum Electronics **1990**, 26, 760;

[30] R. K. Yadav, J. Aneesh, R. Sharma, M. Salvi, J. Jayabalan, H. Jain, K. V. Adarsh, Journal of Applied Physics **2019**, 125, 025702.

[31] Q. Bao, Zhang, H. , Wang, Y. , Ni, Z. , Yan, Y. , Shen, Z. X., Loh, K. P. and Tang, D. Y., Adv Funct Mater **2009**, 19, 3077.

[32] C. Maddi, F. Bourquard, V. Barnier, J. Avila, M. C. Asensio, T. Tite, C. Donnet, F. Garrelie, Scientific reports **2018**, 8.